Migration and transformation of soil mercury in a karst region of southwest China: Implications for groundwater contamination

Jicheng Xia [a, c], Jianxu Wang [a], Leiming Zhang [b], Xun Wang [a], Wei Yuan [a], Tao Peng [a, d], Lirong Zheng [e], Weijun Tian [a, c], Xinbin Feng [a*]

[a] State Key Laboratory of Environmental Geochemistry, Institute of Geochemistry, Chinese Academy of Sciences, Guiyang 550081, China

[b] Air Quality Research Division, Science and Technology Branch, Environment and Climate Change Canada, Toronto, M3H5T4, Canada

[c] University of Chinese Academy of Sciences, Beijing, 100049, China

[d] Puding Karst Ecosystem Research Station, Chinese Academy of Sciences, Puding, 562100, China

[e] Beijing Synchrotron Radiation Facility, Institute of High Energy Physics, Chinese Academy of Sciences, Beijing 100049, China

* Corresponding author.

E-mail address: fengxinbin@vip.skleg.cn

Abstract

Guizhou Province is located in the heart of a karst zone in southwest China, which is one of the largest karst areas in the world. Given the fragile surface ecosystem and highly developed underground karst structure, the migration and transformation of soil Hg may impact groundwater quality in karst environments with high Hg background concentrations. This study examines the vertical migration and transformation of soil mercury (Hg) in two karst catchments, Huilong and Chenqi, with the former containing high Hg contents associated with mineralization and the latter representing regional background Hg. The results show that the soil Hg pool in the Huilong catchment was as high as 44.4±4.2 g m^{-2}, whereas in the Chenqi catchment was only 0.17±0.02 g m^{-2}. Compared with farmland soil, forest soil showed a significant loss of Hg. The results of L_3 X-ray absorption near edge structure of Hg indicated that α-HgS, the primary mineral of Hg ore, gradually changed to other mineral types

during soil formation. In Huilong catchment, the proportion of organic bound $Hg(SR)_2$ out of total Hg decreased from 44.0% to 20.3% when soil depth increased from 10 cm to 160 cm in farmland soil profile and from 39.3% to 34.5% in forest soil profile, while the proportion of ionic Hg increased with soil depth, from 4.2% to 10.7% in the farmland soil profile and from 6.7% to 11.6% in the forestland soil profile. Results from the triple-mixing isotope model show that soil Hg accounts for more than 80% Hg in groundwater in the two catchments. Results from this study indicate potential risks of soil Hg entering into groundwater in this karst area.

Keywords: groundwater contamination, Hg speciation, Hg stable isotopes, karst catchment, land use type

1. Introduction

Mercury is one of the most toxic heavy metal pollutants and can be transported globally by atmospheric processes (Barkay and Wagner-Dobler 2005, Driscoll et al. 2013). Karst ecosystems with high Hg background concentrations play a unique role in the global Hg biogeochemical cycle, especially through fast flow into aquifers and associated risks of groundwater contamination (Chorover et al. 2007, Hartmann et al. 2021, Xia et al. 2021a). The global Hg mineralization zone and karst concentrated area are highly overlapping in southwest China (see Figs. S1 & S2) (Goldscheider et al. 2020, Gustin et al. 1999). China possesses the largest area of karst terrain in the world, and nearly half of the karst landforms in China are distributed in the southwestern part of the country (Huang et al. 2008)). The karst region of southwest China covers an area of 6.2×10^4 km^2 and is located on the global Hg mineralization belt, a region containing the majority of the Hg ore deposits in China. For example, Guizhou Province in this region, the most important Hg production base in China, possesses an estimated Hg reserve of 880,000 tons, accounting for about 78% of the national total (Qiu et al. 2009). The area is characterized by low temperature metallogenic ores

associated with numerous exposed low-temperature hydrothermal deposits. The mining and smelting of Hg and other mineral resources release large quantities of Hg to the surface environment.

Mercury contents in surface (0–25 cm depth) and deeper soils in the karst region of southwest China are 3–5 times higher than those in the other regions of China, largely due to the region's high geochemical background Hg levels (Nie et al. 2019). The high background Hg contents associated with the region's contiguous karst landforms combined with extensive agricultural activities may negatively impact the region's function as an important ecological barrier that protects the middle and upper reaches of the Yangtze and Pearl Rivers. Specifically, excessive agricultural and mining activities may exacerbate the release of Hg into the atmosphere, water and soil environments, seriously affect the environmental quality and agricultural product safety of karst areas. In fact, human activities and other factors that enhanced soil erosion have resulted in an 84% increase in the loss of Hg from 1990 to 2010 in the karst areas of southwest China (Liu et al. 2019b). A better understanding of the biogeochemical cycling of Hg in the karst ecosystem is urgently needed in order to sustain future agricultural development while maintaining a health ecological environment.

Vegetation plays a key role in the biogeochemical cycling of Hg in terrestrial ecosystems. On the global scale, forest ecosystems are a net sink of atmospheric Hg, which absorb about 1,180 tons of Hg from the atmosphere annually (Wang et al. 2016). Agricultural cultivation strongly perturbs the biogeochemical cycling of Hg in terrestrial ecosystems. Fertilization with chemical fertilizers and livestock manure and application of straw to the ground surface represent additional sources of soil Hg in farmlands, while crop harvesting removes Hg from soils, but brings non-negligible Hg exposure health risks to residents in areas with high Hg background concentrations (Xia et al. 2021a). The contradiction between humans' demand for agricultural cultivation and shortage of cultivated land has been long last in the karst areas of southwest China. Large-scale conversion of bare lands to sloping cultivated lands with low

yield has enhanced soil erosion. Some of these converted agricultural lands were later abandoned due to the movement of the rural people into urban living. Guided by the government policy of building a green environment, the vegetation coverage in the karst areas has increased in recent years. For example, the forest coverage in Guizhou province has increased from 30% of the land area in 1998 to 60% in 2020. Such big land use change likely has impacts on Hg biogeochemical cycling in terrestrial ecosystems as well as to underground water quality.

The underground drainage network in the karst area is highly developed, while the thickness of the soil is relatively thin, limiting the region's capacity to resist environmental damage (Xiao et al. 2021). Given the combined traits of an ecologically fragile karst ecosystem and high Hg background levels, the main factors controlling the migration of soil Hg and its transformation under different land use conditions in karst areas need to be better understood. These factors may play an important role in determining and preventing the risk of groundwater Hg pollution in karst areas (Bavec and Gosar 2016, Bollen et al. 2008). While we have a reasonably good understanding of the mass balance of Hg on the catchment scales (Fig. S5&S6), we know little about the fate of soil Hg. To fill this knowledge gap, there is a need to distinguish the behavior of soil Hg in the hydrological process of rainfall infiltration into groundwater. Considering the unique surface-underground dual water flow structure in karst areas, soil Hg distribution, speciation, stable isotope composition can provide important information to explore the sources of groundwater Hg through quantifying soil Hg pool and vertical migration.

This study used water extraction and synchrotron radiation technology to assess the migration and transformation of soil Hg in karst catchments mediated by land use types, and to determine the main controlling factors for the transformation of soil Hg speciation under various conditions. Particularly, Hg stable isotope composition in precipitation, soil, runoff and associated environmental media were analyzed to understand the soil Hg fate in karst

ecosystem. Mercury in soil profiles under different geological background conditions and land use types was analyzed in detail in terms of Hg distribution, speciation and stable isotope composition to better understand the vertical migration and transformation of soil Hg and its potential impacts to groundwater in karst areas. Knowledge gained in this study is useful for developing future land use management and Hg emission control policies in order to sustain future agricultural development while maintaining a healthy ecological environment.

2. Materials and Methods

2.1 Sites descriptions

The two karst catchments in southwestern China, Huilong and Chenqi, were selected in a previous study to assess the source and sink of Hg using a mass balance approach (Xia et al. 2021a). The same two catchments were also selected in the present study to investigate the migration and transformation of soil Hg under different land use. Briefly, the Huilong catchment is located in the southwestern part of Guizhou Province, whereas the Chenqi catchment is located in the central part of the province (Fig. S3), and they are underlain by detrital sandstone and limestone, respectively (Sun et al. 2012, Zhao et al. 2010). Mercury mining in the Huilong catchment continued for about 350 years and ceased in the 1950s, but there are no known Hg deposits in Chenqi (Wang et al. 2005). These two catchments are representative of the region, with the former having higher and the latter having lower Hg (or background) levels. More information about these two catchments can be found in Xia et al. (2021a).

2.2 Sampling and measurement

The locations for soil profile sampling were selected based on the distributions of forests- and farmlands within the catchment. Two locations were selected within each catchment, one for forest soil and another for agricultural soil. Soil and bedrock sampling were performed

with a circular knife/geological hammer from top to bottom to avoid contamination. The soil and bedrock samples were put into sample bags, numbered, and shipped to the laboratory for drying at 40℃. The soil samples were weighed and recorded, and then the visible plants and larger stones higher than 2 mm were removed from the samples (Fernández-Martínez et al. 2015, Shaheen and Rinklebe 2018). After grinding, the soil and bedrock samples were screened through a 200-mesh sieve. The materials were then separated and recorded for further chemical analysis. An Hg analyzer DMA80 (Milestone Ltd. Italy) was used to determine the total Hg content in the collected soil and bedrock samples. The method's detection limit is 0.01 ng g^{-1}. The average relative standard deviation for the duplicate analyses of Hg was 4.7%. Matrix spiked recoveries ranged from 92% to 105% (mean=97%, n=6). The equipment blank for Hg in liquid samples was 0.05 ± 0.01 ng L^{-1} (n=6). The soil reference material GBW07405 was used for soil analytical quality control. The measured average Hg content of the reference materials was 0.27 ± 0.09 mg kg^{-1} (n=6), which was comparable to the certified value of 0.29 ± 0.04 mg kg^{-1}. The relative percentage differences between the sample replicates were <7%.

The sampling and measurement for throughfall, rainfall, surface runoff and groundwater were similar to those described in detailed addressed in Xia et al. (2021a). Two sites in Chenqi and three sites in Huilong catchments were established to collect monthly throughfall (the portion of rainfall which falls to the forest floor from the canopy) from August 2018 to July 2019 (excluding for the dry months). One site at each catchment was established to collect rainfall (open field precipitation) during the same period as for throughfall. A 1.2 m^2 rain board covered with poly tetra fluoro ethylene (PTFE) was placed 0.6 m above the ground to collect rain samples. To avoid possible interference of litterfall and insect debris, a plastic bag was used to cover the rain board during the non-sampling period, and this bag was opened at the start and closed at the end of precipitation. Sampling of surface runoff in each catchment was conducted above the surface converges of runoff, and underground runoff was

conducted in water heads of underground runoff at low terrain. Monthly surface runoff and underground runoff samples were collected in each catchment during the same period as for throughfall. A 5 L brown borosilicate glass bottle was used to collect the water sample. The collected water samples were filtered through a cellulose membrane (0.45-μm pore size, 47-mm diameter, Durapore®, Millipore) into clean and marked brown borosilicate glass bottles, spiked with HCl (final concentration 0.5% (v:v)), oxidized by 50 ml BrCl (0.2 M) for 24 hours, pre-reduced by 20 ml $NH_2OH{\cdot}HCl$ (3.6 M), then reduced with 40 mL $SnCl_2$ (1.05 M) to reduce aqueous Hg^{2+} to Hg^0. The reduced Hg^0 was blown out for 1 hour at a flow rate of 2.5 L min^{-1} and collected by a chlorine-impregnated activated carbon (ClC) trap (Li et al. 2019).

Bedrock, soils and ClC pre-enriched samples were thermal released by two-stage temperature-controlled tubular muffle furnace for isotopic analysis. Mercury released by thermal decomposition was treated with 5 ml of 40% aqua regia absorption liquid capture (Demers et al. 2013, Jiskra et al. 2017). The capture solution was stored in a refrigerator at 4°C prior to Hg isotope analysis. Mercury concentration of the absorbing liquid was determined according to the method of USEAP 1631 with a Hg analyzer Tekran 2500 (Tekran Ltd, CA), and the detection limit of this method was 0.2 ng L^{-1}. The method recoveries of pretreatment were tested using standard reference materials BCR-482 (480±20 μg kg^{-1}) and GSS-4 (590±50 μg kg^{-1}), which were 92.1±3.5% (n=6) and 94.5±4.7% (n=6), respectively.

2.3 Water extracted soil Hg

Approximately 0.4 g of soil sample was placed in a centrifuge tube, and then 35 ml of Milli-Q water (18.2 MΩ) was added. Three replicates per sample. These tubes were then shaken at room temperature for 20 hours, and centrifuged at 5000 rpm for 20 minutes to separate the supernatant. The residue was washed and centrifuged with 5 ml water, and the supernatant was separated and combined with the supernatant obtained in the previous step.

The supernatant was subsequently filtered prior to analysis to determine the quantity of Hg that was in water extracted soil Hg (Bloom et al. 2003, Reis et al. 2014). Mercury concentrations in the extracted solutions were analysed by cold vapor atomic fluorescence spectrometry (Tekran® 2500, refer to the USA EPA Method 1631).

2.4 X-ray absorption near-edge structure spectrum of Hg L_3

About 0.1 g of the sieved soil or bedrock sample was placed into a special tablet press (FW-4, Tianguang Instruments, China) to create a sample pellet, Φ=1 cm. The reference compounds selected in this study were based on the existing literature pertaining to soil and Hg components (Terzano et al. 2010, Yin et al. 2016) and included cinnabar (α-HgS), metacinnabar (β-HgS), synthetic organic bound Hg ($Hg(SR)_2$), nano β-HgS and ionic Hg ($HgCl_2$). The method used to determine the synthetic organic bound Hg ($Hg(SR)_2$) and nano-β-HgS was detailed in Liu et al. (2019a). The experiment was conducted at the 1W1B line station of the Beijing Synchrotron Radiation Facility (BSRF). The basic experimental parameters were set at 2.5 GeV of electron energy, 250 mA of electron current, and an energy resolution (ΔE/E) of $1\text{-}3\times10^{-4}$. For Hg L_3-edge XANES spectroscopy analyses, an energy range of 12.18-12.58 KeV was used to acquire the spectra. Data for Hg reference compounds were collected in transmission mode (Hg content>5%), and for sample pellets in fluorescence mode using a 19-element high-purity Ge solid-state detector under ambient conditions (soil matrix; 15 mg kg^{-1}<Hg content<0.1%). Data normalization (background correction) and linear combination fitting (LCF) were performed with the IFEFFIT software package (Ravel and Newville 2005). The Hg L_3-edge XANES spectra of the standards and samples were plotted with the energy ranged between 12.20 and 12.58 KeV, as described in Wang et al. (2020).

2.5 Determination of Hg stable isotope composition

Before determination of Hg stable isotope composition, the Hg solution was diluted to 1 ng mL^{-1}. The preconcentration recoveries of BCR-482 (480±20 μg kg^{-1}, moss reference

standard) and samples were all in the range of 95%-103%. The Hg isotopic composition was determined by a Nu II multi-receiver plasma mass spectrometer (Nu Instruments, UK) with a gas-liquid separation system HGX-200 (Teledyne CETAC Technologies, USA) and a desolvation nebulizer (CETAC Ardius) (Yin. et al. 2010). Gaseous elemental Hg was generated online from Hg standard sample or test sample by using $SnCl_2$ (3%) as the reducing agent of Hg. Instrument mass bias correction was performed using internal standards (NIST 997) and external standards (NIST 3133).

Mercury isotope mass-dependent fractionation (MDF) is expressed as δ(‰) and is calculated as follows:

$$\delta^{202}Hg(‰) = 1000 \times [(^{202}Hg/^{198}Hg_{sample})/(^{202}Hg/^{198}Hg_{NISTSRM3133}) - 1] \quad (1)$$

The mass-independent fractionation (MIF) of Hg isotopes is represented by Δ(‰), and is calculated as follows:

$$\Delta^{199}Hg\ (‰) \approx \delta^{199}Hg - 0.2520 \times \delta^{202}Hg \quad (2)$$

$$\Delta^{200}Hg\ (‰) \approx \delta^{200}Hg - 0.5024 \times \delta^{202}Hg \quad (3)$$

$$\Delta^{201}Hg\ (‰) \approx \delta^{201}Hg - 0.7520 \times \delta^{202}Hg \quad (4)$$

$$\Delta^{204}Hg\ (‰) \approx \delta^{204}Hg - 1.4930 \times \delta^{204}Hg \quad (5)$$

One UM-Almadén solution was inserted as an internal standard for every 10 samples. In order to evaluate whether the pretreatment process such as pyrolysis-pre-enrichment will lead to obvious isotopic bias, the reference standard materials BCR-482 and GSS-4 were determined several times during the sampling period. Results of UM-Almaden ($\delta^{202}Hg$ = –0.53 ± 0.08‰, $\Delta^{199}Hg$ = –0.01 ± 0.05‰, $\Delta^{201}Hg$ = –0.02 ± 0.07‰, 2 SD, n = 8) and BCR-482 ($\delta^{202}Hg$ = –1.55 ± 0.09‰, $\Delta^{199}Hg$ = –0.58 ± 0.06‰, $\Delta^{200}Hg$ = –0.01 ± 0.03‰, $\Delta^{201}Hg$ = –0.59 ± 0.08‰, 2 SD, n = 3) are consistent with previously reported values, indicating that both the instrument precision and the sample pretreatment method were reliable (Blum and Bergquist 2007).

No significant odd or even MIF occurred during dissolution, but MDF was present (Drott et al. 2013, Wiederhold et al. 2015). Therefore, for the hydrological process that only includes leaching, dissolution and scrubbing, Δ^{199}Hg and Δ^{200}Hg can be used to calculate the end member ratio. With two degrees of freedom, the contribution ratio of the three end members can be calculated at the same time. A triple-mixing isotope model was thus used to quantify the contribution of potential groundwater Hg inputs (e.g., rainfall Hg, throughfall Hg and soil Hg). Monte Carlo simulation was applied to generate one million groups of Δ^{199}Hg and Δ^{200}Hg, which randomly ranging from Mean –SD to Mean +SD (Wang et al. 2019). The fraction ratio (f_i) is estimated as the average of these solutions, which is in the range of 0–1, based on one million times of solutions of Eqs. (6-8).

$$f_1\times\Delta^{199}Hg_1+f_2\times\Delta^{199}Hg_2+f_3\times\Delta^{199}Hg_3=\Delta^{199}Hg_{groundwater} \quad (6)$$

$$f_1\times\Delta^{200}Hg_1+ f_2\times\Delta^{200}Hg_2+f_3\times\Delta^{200}Hg_3=\Delta^{200}Hg_{groundwater} \quad (7)$$

$$f_1+f_2+f_3=1 \quad (8)$$

2.6 Soil Hg migration coefficient

The migration coefficient (*MC*) can be used to describe the migration and enrichment characteristics of Hg in the soil profile relative to the bedrock (Nesbitt 1979, Sun et al. 2019), and was calculated as:

$$MC = \frac{C_{S-Hg}}{C_{S-Zr}} \times \frac{C_{R-Zr}}{C_{R-Hg}} - 1 \quad (11)$$

where $C_{S\text{-}Hg}$ and $C_{S\text{-}Zr}$ are the Hg and zirconium content in the soil and $C_{R\text{-}Hg}$ and $C_{R\text{-}Zr}$ are those in the bedrock, respectively. Zirconium was chosen as a reference element because of zircon's excellent stability to weathering results from its exceptionally low solubility in aqueous solutions (Santos et al. 2019). Soil and bedrock zirconium contents were analysed using inductively coupled plasma mass spectrometry, as detailed in Xia et al. (2021b). A $MC>0$ indicates that the sampling point is enriched in Hg during the soil-forming process, while a $MC<0$ indicates the Hg in the sampling point is depleted.

3. Results and Discussion

3.1 Distribution of Hg in soil profiles

The soil Hg contents in the farmland and forested sections of the Huilong catchment were 97.9±51.3 mg kg^{-1} and 20.0±4.9 mg kg^{-1}, respectively, and those in the Chenqi catchment were 0.16±0.05 mg kg^{-1} and 0.21±0.19 mg kg^{-1}, respectively. Soil Hg content in the farmland section of the Huilong catchment slightly decreased with soil depth beneath the H-A-O (Fig. 1a). The soil closer to the surface is affected more by agricultural practices (such as fertilization) as well as atmospheric deposition of Hg (Ma et al. 2022). Soil Hg content gradually increased from the bottom of the H-A-O to the H-A-B, likely due to the downward leaching and migration of Hg from the upper soil layer. Soil Hg content increased significantly with soil depth in the H-A-C, presumably because of its proximity to the parent material that possessed relatively high Hg concentrations. Soil Hg content in the forestland section of the Huilong catchment decreased with soil depth from the H-F-O to H-F-A (Fig. 1b). Mercury leaching was likely related to the layers with low soil pH (between 4 and 5). At greater soil depths, Hg began to accumulate and soil Hg content increased.

Soil Hg content in the farmland section of the Chenqi catchment was relatively high in the C-A-O (Fig. 1c), possibly because of Hg input from agricultural ploughing and atmospheric Hg deposition. From the lower part of the C-A-O to the C-A-A, a portion of easily dissolved Hg migrated downward through soil seepage, and was subsequently fixed in the C-A-B. Soil Hg content changed little with soil depth in the bottom soil, which may be related to the low geological background Hg in this area of the Chenqi catchment and absence of exogenous Hg input or human activities. Soil Hg content in the forestland section of the Chenqi catchment exhibited high concentrations in the C-F-O (Fig. 1d), which was mainly due to litterfall Hg input. Soil Hg content decreased with soil depth in the C-F-A due to Hg leaching. Soil Hg content increased with soil depth in the C-F-B due to the migration of Hg from the upper soil layer.

3.2 Mercury migration and accumulation in the karst soil profiles

In this study, the migration and accumulation of Hg in the farmland and forestland soil profiles of the Huilong and Chenqi catchments were characterized using a migration coefficient (*MC*) (Fig. 2a). The farmland soil profile within the Huilong catchment possessed two distinct ranges of *MC* values: *MC* >0 and *MC* <0. *MC* is in the range of -0.9 – 0.0 at soil depths of 0–80 cm and 130–180 cm, indicating that soil Hg at these depths is relatively depleted. This suggests that the shallow and deep seepage of water through the soil has leached the soil Hg within these two soil layers (Abu-Dieyeh et al. 2019). In addition, Hg may have been lost from the soil surface by interfacial Hg exchange with the atmosphere. Since the background soil Hg concentrations are as high as several hundreds of mg kg^{-1} in this area, the magnitude of the interfacial Hg exchange between soil and atmosphere interface is likely large and result in Hg loss from soil (Qiu et al. 2006). *MC* is in the range of 0.0 – 0.9 at soil depths of 80 –130 cm, indicating that soil Hg at these depths is relatively enriched. Mercury enrichment may be due to the downward transport of Hg from the upper layer and its subsequent redeposition.

For the forest soil profile of the Huilong catchment, soil Hg was relatively depleted in general with *MC* being in the range of -0.75 – 0.0 (Fig. 2b). In the organic layer (0 – 20 cm soil depth), the degree of Hg loss was limited (*MC*: -0.54 – -0.45), likely due to the release of Hg from leaf litterfall degradation that supplements the soil Hg. The degree of Hg loss is relatively large between 40–60 cm depth (*MC*: -0.75 – -0.71) due to strong leaching and no effective supplementation of Hg. The depletion of Hg decreases at depths closer to the bedrock, likley due to higher Hg concentrations derived from the bedrock and retained in the regolith and semi-regolith near the bedrock.

In the farmland soil profile of the Chenqi catchment, soil Hg was enriched at all depth, with *MC* being in the range of 0 – 1.64 (Fig. 2c). The farmland is located in lower topographic

areas of the catchment, and therefore continuously receives and accumulats Hg from eroded soil transported by surface runoff from areas of higher terrain and steeper slopes. The enrichment of Hg in the topsoil may also be related to atmospheric deposition and/or agricultural inputs. In the accumulation layer of the soil profile between 30–60 cm in depth, *MC* increased significantly, reaching values as high as 1.6. The very high *MC* values at these depths indicate highly enriched Hg, presumably due to leaching from overlying soil (Santos-Frances et al. 2011, Teršič et al. 2014).

Soil Hg in the forest soil profile of the Chenqi catchment was relatively depleted in general (Fig. 2d), with *MC* being in the range of −0.7 – 0.0. In the organic layer (0 and 20 cm depth), the degree of Hg loss was relatively weak, possibly because of supplemental Hg released from leaf litterfall degradation (Silva-Filho et al. 2006). Soils between 20–40 cm depth exhibited a large degree of Hg loss (Fig. 2d), suggesting strong leaching while with limited Hg supplementation. The depletion of Hg decreases at depths closer to the bedrock, which may be because the soil at the bottom of the profile was not fully developed, limiting Hg migration at this depth.

In general, farmland soils in catchment depressions were close to 2 meters in thickness. Mercury in the deep soils shows varying degrees of depletion or enrichment depending on the superposition of factors such as the contributions of Hg from bedrock weathering, soil seepage and leaching, among others. Considering that lower pH should enhance Hg leaching (Soleh Setiyawan et al. 2020), soil pH might have also played an important role in shaping the soil Hg profile, knowing that soil pH of Huilong catchment is between 4.24 and 6.98 and that of Chenqi catchment is between 6.93 and 7.61 (Table S2). The thickness of the forest soil layer on the hillside is less than 1 meter. The thin soil layer could be caused by prominent soil erosion and large hill slopes in the karst area, both factors were conducive to Hg leaching through surface runoff and internal soil seepage. The reduced Hg loss in the organic soil layer should be related to the replenishment of soil Hg from litterfall input (Xia et al. 2021a).

338

339 *3.3 Water extracted Hg*

340 The water extracted soil Hg contents were 51.9-1742 μg kg^{-1} and 0.88-10.8 μg kg^{-1},
341 accounting for 0.24-6.3% and 0.73-6.4% of the total Hg in Huilong and Chenqi catchment,
342 respectively (Fig. 3).

343 The contents and proportions of water extracted Hg increased from the H-A-O to the H-A-
344 A, and decreased to the H-A-B in the farmland soil profile of the Huilong catchment, and
345 increased from the H-A-O to the H-A-A in the forestland soil profile of the same catchment
346 (Fig. 3a). In the Chenqi farmland soil profile (Fig. 3b), the contents and proportions of water
347 extracted Hg increased from the C-A-O to the C-A-A, and decreased to the C-A-B. In the
348 forestland soil profile, the contents of water extracted Hg decreased from C-F-O to C-F-B,
349 while the proportions of water extracted Hg increased first, and then decreased. There was an
350 obvious similarity among these four profiles, in that the water extracted Hg had a significant
351 upward trend in the leaching layer. A similar phenomenon has also been reported in previous
352 studies. This is because most soluble Hg in soil occurs in the speciation of non-reactive
353 complex binding, and it is highly likely that Hg binds to soluble humic matter (Teršič et al.
354 2014). It has also been suggested that nano Hg containing particles or colloids may be
355 released during leaching (Gray et al. 2004).

356

357 *3.4 Mercury speciation in the soil profiles determined by XANES*

358 Data obtained from the synchrotron radiation near-side absorption spectrum for the
359 farmland soil profile in the Huilong catchment (Fig. 4) showed that organically bound Hg
360 decreased from the surface H-A-O to the H-A-A, and to the H-A-B. The proportion of
361 $Hg(SR)_2$ in these three layers was 44.0%, 23.2% and 20.3%, respectively, similar to those of
362 organically bound Hg extracted by the BCR. The high proportion of organically bound Hg in
363 the cultivated layer of the soil may be related to long-term agricultural farming activities,

including the addition of straw and fertilization to the farm field. The application of livestock manure may be particularly important. In the Huilong catchment, the annual average yields of corn stalks and barley stalks were as high as 20250 and 6750 kg ha^{-1} yr^{-1}, while their Hg contents were 0.32±0.05 mg kg^{-1} and 0.15±0.03 mg kg^{-1}, respectively (Xia et al. 2021a). A portion of the harvested straw is naturally degraded and incorporated into the soil as it is returned to the fields. The remaining portion of straw is usually recycled by farmers to feed livestock, and the resulting farmyard manure is applied to the farmland. Thus, while the soil fertility of the cultivated layer is improved, the content of organically bound Hg in the soil is always maintained at a high level. $Hg(SR)_2$ is potentially bioavailable, especially when the soil is acidic. Soil Hg in the form of $Hg(SR)_2$ could increase Hg contents in crop products, and subsequently increase the risk of Hg exposure by local residents consuming products. Meanwhile, $Hg(SR)_2$ in soil could also increase the possibility of Hg conversion to ionic Hg, which will increase the potential downward migration of Hg from the upper soil layers by leaching.

The proportion of ionic Hg increased gradually with soil depth from 4.2% to 6.9%, and then to 10.7% (Fig. 4). The acidic nature of the soil at Huilong likely allows for significant leaching, resulting in continuous accumulation and increasing proportions of ionic Hg from the top to bottom of the soil profile. This trend is consistent with observed downward increase in organic matter content (Fig. 4). The ionic Hg that can be combined and fixed by the organic matter decreases, suggesting that with continued leaching of ionic Hg the sorption capacity of the organic matter becomes saturated, allowing Hg to be transported to greater depths (Leterme et al. 2014, McLagan et al. 2022). A considerable amount (ranging from a few percent to a dozen percent) of ionic Hg has been observed in the soils of several world-famous Hg mining districts (such as Almadén, Asturias (Spain), Idria (Slovenia) and Wanshan (China)) (Esbri et al. 2010, Yin et al. 2016). Soils characterized by high Hg background content and intensive soil leaching of ionic Hg increases the risk of the downward

migration of soil Hg to groundwater. Note that it is not suitable to directly compare the ionic Hg determined by XANES with water extracted Hg due to their significant differences caused by matrix and particle size and/or by crystallinity effect, which affect the apparent solubility of Hg phase (Kim et al. 2003).

The proportion of α-HgS increases toward the deep soil from 8.5% to 9.3%, and to 21.0%. α-HgS was the main component of natural Hg ore. The content of this form of Hg tends to decrease with soil formation. It may be transformed to other forms of Hg by biologically-mediated weathering (Gómez-Armesto et al. 2020, Wu et al. 2017). The closer the soil is to the surface, the stronger the weathering is and the more primary minerals are degraded, thereby reducing the portion of soil Hg as α-HgS (Bourdineaud et al. 2020).

The proportions of β-HgS in the H-A-O and H-A-A were 13.6% and 9.3%, respectively, whereas those of nano β-HgS were 26.8% and 50.0%, respectively. A possible factor producing the opposite trends between β-HgS and nano β-HgS is the transformation of nano β-HgS, which is an amorphous Hg sulfide. Soil weathering, especially in the cultivated layer that is strongly disturbed by farming, may promote the transformation of Nano β-HgS into more stable β-HgS.

In the forestland of the Huilong catchment, the proportion of organically bound Hg ($Hg(SR)_2$) declined slightly from 39.3% in the H-F-O to 34.5% in the H-F-A. This observed downward trend may be due to the accumulation of Hg in the surficial soil organic layer of the forestland from degradation of litterfall where the soil organic matter is constantly being renewed. The Hg flux from litterfall input in the Huilong catchment was estimated to be 129±85.3 μg m^{-2} yr^{-1} (Xia et al. 2021a). Most of the Hg derived from the degradation of litterfall will be incorporated into the soil, allowing organically bound Hg in the surface soil to be maintained at a relatively high level. The proportion of ionic Hg increased significantly, from 6.7% in the H-F-O to 11.6% in the H-F-A. The observed trend may be controlled by soil pH and SOM as described for the farmland soil. It may also be related to the greater moisture

content of the forestland soils, which have a natural advantage in water retention in comparison to adjacent non-forestlands (Monteiro Venturini et al. 2022). The tall forest canopy reduces solar radiation reaching to the surface, thereby reduces temperature and evaporation rate of soil water, which leads to higher soil moisture content that is conducive to leaching. In contrast to the farmland soil profile, the proportion of α-HgS in the forestland profile initially decreases by a large amount and then increases at greater depths (Fig. 4). The sharp decrease may be due to the lack of a plough layer in the surface soil that has been disturbed by anthropogenic activities over the years. In addition, the top layer of the forest was characterized by litterfall, and there was more bedrock in the bottom layer. α-HgS in the A-horizon is affected by its higher water content and by its well-developed plant root system that strengthens the effects of soil weathering and leaching. Thus, the primary minerals in this layer were α-HgS, which would be transformed into other forms of secondary minerals under strong weathering and leaching conditions. The limited weathering within the H-F-C results in a large proportion of the primary mineral α-HgS, which accounts for 85.4% of the total, leaving the remaining 16.9% as β-HgS.

In general, SOM was closely related to the oxidizable Hg. In the process of soil formation, the main primary mineral α-HgS of the Hg ore gradually changed to other mineral types. As the soil depth increases, the proportion of $Hg(SR)_2$ decreases, while the ionic Hg tends to increase. It is worth to note that the increasing tendency of ionic Hg with increasing soil depth implies that the risk of soil Hg entering groundwater is high in the karst areas with high Hg background. Therefore, both soil Hg profile and possible migration of Hg to groundwater need to be closely monitored in order to develop effective control measures to prevent soil Hg pollution to groundwater.

3.5 Mercury isotopic signatures in karst hydrological processes

The Hg isotopic signatures of rainfall in Huilong were δ^{202}Hg=-1.00±0.61‰, Δ^{199}Hg=0.48±0.19‰ and Δ^{200}Hg=0.13±0.05‰ (n=8), and those of throughfall were δ^{202}Hg=-1.77±0.47‰, Δ^{199}Hg=-0.06±0.11‰ and Δ^{200}Hg=0.02±0.03‰ (n=8) (Fig. 5a). The Hg isotopic signatures of rainfall in Chenqi were δ^{202}Hg=-0.42±0.14‰, Δ^{199}Hg=0.29±0.17‰ and Δ^{200}Hg=0.12±0.03‰ (n=5), and those of throughfall were δ^{202}Hg=-1.44±0.60‰, Δ^{199}Hg=-0.07±0.16‰ and Δ^{200}Hg=0.07±0.04‰ (n=11) (Fig. 5b). Note that the Hg isotopic signatures of natural precipitation in the global background area were δ^{202}Hg=-0.57±0.48‰, Δ^{199}Hg=0.44±0.23‰ and Δ^{200}Hg=0.25±0.19‰ (Chen et al. 2012, Demers et al. 2013, Donovan et al. 2013). The MDF of Hg isotopes in the Chenqi catchment was slightly negative, and the MIF of Hg isotope was significantly negative by about 0.2‰, which was likely due to the significantly higher Hg concentration in the precipitation in Chenqi (7.9–26.0 ng L^{-1}) compared to those of the forest precipitation in the global background area (5.9–19.0 ng L^{-1}) (Fu. et al. 2010, Schwesig and Matzner 2000, Xia et al. 2021a). The Hg isotopic signatures observed in Chenqi reflect the influence of anthropogenic Hg sources that have negative δ^{202}Hg, and close to 0 Δ^{199}Hg and Δ^{200}Hg (Blum et al. 2014, Kwon et al. 2020, Tsui et al. 2020). Besides, a portion of the Hg isotopic signatures of the throughfall was inherited from those of the vegetation canopy due to the washout of particulate Hg adsorbed on the surface of leaves and trunks by throughfall. The Hg isotopic signatures of the vegetation canopy were characterized with negative δ^{202}Hg and Δ^{199}Hg and close to 0 Δ^{200}Hg (Demers et al. 2013, Yu et al. 2016). In conclusion, the Hg isotopic signatures of the forest soil do not have positive Δ^{200}Hg, and the Δ^{199}Hg signal was further diluted. Such a finding was of great significance for tracing the Hg cycle in the hydrological process of the karst area.

The Hg isotopic signatures of bulk soil were δ^{202}Hg=-0.29±0.24‰, Δ^{199}Hg=0.01±0.06‰ and Δ^{200}Hg=0.02±0.03‰ (n=11) in Huilong catchment (Fig. 5a), and were δ^{202}Hg=-1.34±0.34‰, Δ^{199}Hg=-0.02±0.06‰ and Δ^{200}Hg=-0.02±0.02‰ (n=7) in Chenqi catchment (Fig. 5b). The Hg isotope composition of bedrock were δ^{202}Hg=-0.79±0.23‰,

467 Δ^{199}Hg=0.05±0.05‰ and Δ^{200}Hg=0.01±0.03‰ (n=3) in Huilong catchment, and were
468 δ^{202}Hg=-0.83±0.05‰, Δ^{199}Hg=0.17±0.07‰ and Δ^{200}Hg=0.04±0.01‰ (n=2) in Chenqi
469 catchment. Compared with Hg isotope composition of bedrocks in the other regions of the
470 world, δ^{202}Hg was usually negative, and both Δ^{199}Hg and Δ^{200}Hg were close to 0 (Obrist et al.
471 2017, Smith et al. 2008). The slightly positive Δ^{199}Hg for carbonate rocks observed in the
472 present study may be related to the material deposition-diagenesis process, but more
473 evidences are needed to confirm this.

474 The Hg isotope composition of surface runoff in Huilong were δ^{202}Hg=-0.66 ± 0.27‰,
475 Δ^{199}Hg=0.16 ± 0.13‰ and Δ^{200}Hg=0.03±0.04‰ (n=5), and those of groundwater were
476 δ^{202}Hg=-0.42 ± 0.15‰, Δ^{199}Hg=0.05 ± 0.07‰ and Δ^{200}Hg=0.03±0.01‰ (n=4) (Fig. 5a). The
477 Hg isotope composition of surface runoff in Chenqi were δ^{202}Hg=-1.10 ± 0.23‰,
478 Δ^{199}Hg=0.06 ± 0.15‰ and Δ^{200}Hg=0.02±0.08‰ (n=5), and those of groundwater were
479 δ^{202}Hg=-1.38 ± 0.21‰, Δ^{199}Hg=-0.02 ± 0.10‰ and Δ^{200}Hg=0.00±0.02‰ (n=6) (Fig. 5b). The
480 Hg isotopes of surface runoff retained the signatures of rainfall to a certain extent, especially
481 the positive Δ^{199}Hg, likely because the surface runoff in this area was formed within a short
482 time after rainfall and then infiltrated rapidly. The Hg isotopes of groundwater were generally
483 consistent with those of soil in the two catchments, suggesting sufficient exchange with soil
484 Hg, including a series of adsorption/desorption processes, after precipitation entering the soil
485 system (McLagan et al. 2022).

486 Using the triple-mixing isotope model, it was estimated that soil Hg, rainfall Hg and
487 throughfall Hg contributed 84 ± 9%, 11 ± 9% and 5 ± 12%, respectively, to groundwater Hg
488 in Huilong, and 88 ± 12%, 5 ± 20% and 7 ± 25%, respectively, in Chenqi. Thus, soil Hg was
489 the main source for groundwater Hg. Surface fissures developed in karst areas and land use
490 types may directly impact rainfall and throughfall Hg input to groundwater.

491

492 *3.6 The implications of soil Hg transformation to karst groundwater safety*

493 Due to the unique dual hydrologic structure of the area's karst system (characterized by
494 both an above ground and underground flow field), the downward migration of soil Hg
495 becomes a potential risk for regional groundwater security in karst areas with high Hg
496 background concentrations, such as in Huilong catchment with a soil Hg pool as high as
497 44.4±4.2 g m^{-2}. Previous research documented that Hg-DOM and ionic Hg have relatively
498 higher vertical mobility in soil (Gai et al. 2016). $Hg(SR)_2$ investigated in the present study has
499 similar chemical properties to those of Hg-DOM reported in literature (Liu et al. 2019a). Fig.
500 6 shows an illustration of Hg migration and transformation in farmland and forest soil profiles
501 in the Huilong catchment based on results from the present study and data reported in Xia et
502 al. (2021a). The present study shows ionic Hg increases with increasing soil depth, and such
503 an increase is stronger in forest soil (from 6.7% to 11.6%) than in farmland soil (from 4.2% to
504 10.7%), while $Hg(SR)_2$ decreases with soil depth, and the trend is stronger in farmlands (from
505 44.0% to 20.3%) than forests (from 39.3% to 34.5%). Soil moisture contents are likely higher
506 in forest soils than farmland soils due to the higher canopy height of forests. The leaching
507 effect of ionic Hg in forest soils is thus stronger, as seen in the stronger trend of its vertical
508 migration. The input of forest litterfall provides continuous replenishment of organic matter in
509 the understory soil, resulting in downward migration of $Hg(SR)_2$. At the catchment scale, Hg
510 input flux from precipitation and output flux through runoff were 20.9±13.3 μg m^{-2} yr^{-1} and
511 21.6±0.93 μg m^{-2} yr^{-1}, respectively (Xia et al. 2021a). Soil Hg speciation and associated high
512 levels of Hg fluxes in various hydrological processes suggest the potential risks of soil Hg
513 migration to groundwater in this karst area. This was consistent with the results of Hg isotope
514 source analysis for groundwater Hg.
515
516 **4. Conclusions**
517 The groundwater Hg was derived mainly from soil in Huilong and Chenqi catchments.
518 The extremely high soil Hg pool suggests a big risk of Hg diffusion to the surrounding

environment in Huilong. From the perspective of the vertical migration of Hg in the soil profiles, a more obvious Hg depletion was observed in the forest soil than the farmland soil. During soil formation, α-HgS, which is the primary Hg ore mineral, is gradually transformed into other mineral types, and this slow transformation process of α-HgS in the soil provides opportunity for groundwater contamination. The proportion of organic bound $Hg(SR)_2$ decreased while the proportion of ionic Hg increased with increasing soil depth. It is particularly noteworthy that the tendency of ionic Hg to increase with soil depth suggests an increased risk of soil Hg entering into groundwater in karst areas with high Hg background. Therefore, the management and remediation of soil Hg pollution in such areas should focus on not only Hg at the soil surface, but also Hg migration to groundwater. Future research should take into account the migration and transformation of Hg in hydrological processes under different land use in karst areas.

Acknowledgement

This work was supported by the Program Foundation of the National Natural Science Foundation of China [41921004, U1612442 and 42107497], the Strategic Priority Research Program of Chinese Academy of Sciences [XDB40000000], and the Guizhou Provincial Science and Technology Projects (QKHJC-ZK[2021]YB227).

References

Abu-Dieyeh, M.H., Alduroobi, H.M. and Al-Ghouti, M.A. (2019) Potential of mercury-tolerant bacteria for bio-uptake of mercury leached from discarded fluorescent lamps. Journal of Environmental Management 237, 217-227.

Barkay, T. and Wagner-Dobler, I. (2005) Microbial transformations of mercury: Potentials, challenges, and achievements in controlling mercury toxicity in the environment. Advances in Applied Microbiology 57, 1-52.

Bavec, Š. and Gosar, M. (2016) Speciation, mobility and bioaccessibility of Hg in the polluted urban soil of Idrija (Slovenia). Geoderma 273, 115-130.

Bloom, N.S., Preus, E., Katon, J. and Hiltner, M. (2003) Selective extractions to assess the biogeochemically relevant fractionation of inorganic mercury in sediments and soils. Analytica Chimica Acta 479(2), 233-248.

Blum, J.D. and Bergquist, B.A. (2007) Reporting of variations in the natural isotopic composition of mercury. Analytical and Bioanalytical Chemistry 388(2), 353-359.
Blum, J.D., Sherman, L.S. and Johnson, M.W. (2014) Annual Review of Earth and Planetary Sciences, Vol 42. Jeanloz, R. (ed), pp. 249-269.
Bollen, A., Wenke, A. and Biester, H. (2008) Mercury speciation analyses in HgCl(2)-contaminated soils and groundwater--implications for risk assessment and remediation strategies. Water Res 42(1-2), 91-100.
Bourdineaud, J.P., Durn, G., Rezun, B., Manceau, A. and Hrenovic, J. (2020) The chemical species of mercury accumulated by Pseudomonas idrijaensis, a bacterium from a rock of the Idrija mercury mine, Slovenia. Chemosphere 248, 126002.
Chen, J., Hintelmann, H., Feng, X. and Dimock, B. (2012) Unusual fractionation of both odd and even mercury isotopes in precipitation from Peterborough, ON, Canada. Geochimica Et Cosmochimica Acta 90, 33-46.
Chorover, J., Kretzschmar, R. and Sparks, L.D. (2007) Soil Biogeochemical Processes within the Critical Zone. Elements 3, 321-326.
Demers, J.D., Blum, J.D. and Zak, D.R. (2013) Mercury isotopes in a forested ecosystem: Implications for air-surface exchange dynamics and the global mercury cycle. Global Biogeochemical Cycles 27(1), 222-238.
Donovan, P.M., Blum, J.D., Yee, D., Gehrke, G.E. and Singer, M.B. (2013) An isotopic record of mercury in San Francisco Bay sediment. Chemical Geology 349-350, 87-98.
Driscoll, C.T., Mason, R.P., Chan, H.M., Jacob, D.J. and Pirrone, N. (2013) Mercury as a Global Pollutant: Sources, Pathways, and Effects. Environmental Science & Technology 47(10), 4967-4983.
Drott, A., Bjorn, E., Bouchet, S. and Skyllberg, U. (2013) Refining thermodynamic constants for mercury(II)-sulfides in equilibrium with metacinnabar at sub-micromolar aqueous sulfide concentrations. Environmental Science & Technology 47(9), 4197-4203.
Esbri, J.M., Bernaus, A., Avila, M., Kocman, D., Garcia-Noguero, E.M., Guerrero, B., Gaona, X., Alvarez, R., Perez-Gonzalez, G., Valiente, M., Higueras, P., Horvat, M. and Loredo, J. (2010) XANES speciation of mercury in three mining districts - Almaden, Asturias (Spain), Idria (Slovenia). J Synchrotron Radiat 17(2), 179-186.
Fernández-Martínez, R., Larios, R., Gómez-Pinilla, I., Gómez-Mancebo, B., López-Andrés, S., Loredo, J., Ordóñez, A. and Rucandio, I. (2015) Mercury accumulation and speciation in plants and soils from abandoned cinnabar mines. Geoderma 253-254, 30-38.
Fu., Feng, X., Zhu, W., Rothenberg, S., Yao, H. and Zhang, H. (2010) Elevated atmospheric deposition and dynamics of mercury in a remote upland forest of southwestern China. Environmental Pollution 158(6), 2324-2333.
Gai, K., Hoelen, T.P., Hsu-Kim, H. and Lowry, G.V. (2016) Mobility of Four Common Mercury Species in Model and Natural Unsaturated Soils. Environmental Science & Technology 50(7), 3342-3351.
Goldscheider, N., Chen, Z., Auler, A.S., Bakalowicz, M., Broda, S., Drew, D., Hartmann, J., Jiang, G., Moosdorf, N., Stevanovic, Z. and Veni, G. (2020) Global distribution of carbonate rocks and karst water resources. Hydrogeology Journal 28(5), 1661-1677.
Gómez-Armesto, A., Méndez-López, M., Pontevedra-Pombal, X., García-Rodeja, E., Moretto, A., Estévez-Arias, M. and Nóvoa-Muñoz, J.C. (2020) Mercury accumulation in soil fractions of podzols from two contrasted geographical temperate areas: southwest Europe and southernmost America. Geoderma 362, 114120.
Gray, J.E., Hines, M.E., Higueras, P.L., Adatto, I. and Lasorsa, B.K. (2004) Mercury speciation and microbial transformations in mine wastes, stream sediments, and surface waters at the Almadén Mining District, Spain. Environmental Science & Technology 38, 4285–4292.
Gustin, M.S., Lindberg, S., Marsik, F., Casimir, A., Ebinghaus, R., Edwards, G., Hubble-Fitzgerald, C., Kemp, R., Kock, H., Leonard, T., London, J., Majewski, M., Montecinos, C., Owens, J., Pilote, M., Poissant, L., Rasmussen, P., Schaedlich, F., Schneeberger, D., Schroeder, W., Sommar, J., Turner, R., Vette, A., Wallschlaeger, D., Xiao, Z. and Zhang, H. (1999) Nevada STORMS project: Measurement of mercury emissions from naturally enriched surfaces. Journal of Geophysical Research: Atmospheres 104(D17), 21831-21844.

Hartmann, A., Jasechko, S., Gleeson, T., Wada, Y., Andreo, B., Barbera, J.A., Brielmann, H., Bouchaou, L., Charlier, J.B., Darling, W.G., Filippini, M., Garvelmann, J., Goldscheider, N., Kralik, M., Kunstmann, H., Ladouche, B., Lange, J., Lucianetti, G., Martin, J.F., Mudarra, M., Sanchez, D., Stumpp, C., Zagana, E. and Wagener, T. (2021) Risk of groundwater contamination widely underestimated because of fast flow into aquifers. Proc Natl Acad Sci U S A 118(20).

Huang, Q.H., Cai, Y.L. and Xing, X.S. (2008) Rocky desertification, antidesertification, and sustainable development in the karst mountain region of Southwest China. Ambio 37(5), 390-392.

Jiskra, M., Wiederhold, J.G., Skyllberg, U., Kronberg, R.M. and Kretzschmar, R. (2017) Source tracing of natural organic matter bound mercury in boreal forest runoff with mercury stable isotopes. Environ Sci Process Impacts 19(10), 1235-1248.

Kim, C., S,, Bloom, N., S, , Rytuba, J., J and Brown, G.E. (2003) Mercury speciation by X-ray absorption fine structure spectroscopy and sequential chemical extractions: a comparison of speciation methods. Environmental Science & Technology Letters 37(22), 5102-5108.

Kwon, S.Y., Blum, J.D., Yin, R., Tsui, M.T.-K., Yang, Y.H. and Choi, J.W. (2020) Mercury stable isotopes for monitoring the effectiveness of the Minamata Convention on Mercury. Earth-Science Reviews 203, 103111.

Leterme, B., Blanc, P. and Jacques, D. (2014) A reactive transport model for mercury fate in soil—application to different anthropogenic pollution sources. Environmental Science and Pollution Research 21.

Li, K., Lin, C.-J., Yuan, W., Sun, G., Fu, X. and Feng, X. (2019) An improved method for recovering and preconcentrating mercury in natural water samples for stable isotope analysis. Journal of Analytical Atomic Spectrometry 34(11), 2303-2313.

Liu, Wang, J., Feng, X., Zhang, H., Zhu, Z. and Cheng, S. (2019a) Spectral insight into thiosulfate-induced mercury speciation transformation in a historically polluted soil. Science of the Total Environment 657, 938-944.

Liu, Zhang, Q., Ge, S., Mason, R.P., Luo, Y., He, Y., Xie, H., Sa, R., Chen, L. and Wang, X. (2019b) Rapid Increase in the Lateral Transport of Trace Elements Induced by Soil Erosion in Major Karst Regions in China. Environmental Science & Technology 53(8), 4206-4214.

Ma, H., Cheng, H., Guo, F., Zhang, L., Tang, S., Yang, Z. and Peng, M. (2022) Distribution of mercury in foliage, litter and soil profiles in forests of the Qinling Mountains, China. Environmental Research 211, 113017.

McLagan, D.S., Schwab, L., Wiederhold, J.G., Chen, L., Pietrucha, J., Kraemer, S.M. and Biester, H. (2022) Demystifying mercury geochemistry in contaminated soil-groundwater systems with complementary mercury stable isotope, concentration, and speciation analyses. Environ Sci Process Impacts.

Monteiro Venturini, A., Silvestre Dias, N.M., Gontijo, J.B., Yoshiura, C.A., da Silva Paula, F., Meyer, K.M., Nakamura, F.M., da Franca, A.G., Borges, C.D., Barlow, J., Berenguer, E., Nusslein, K., Mazza Rodrigues, J.L., Bohannan, B.J.M. and Tsai, S.M. (2022) Increased soil moisture intensifies the impacts of forest-to-pasture conversion on methane emissions and methane-cycling communities in the Eastern Amazon. Environmental Research, 113139.

Nesbitt, H.W. (1979) Mobility and fractionation of rare earth elements during weathering of a granodiorite. Nature 279, 206-210.

Nie, L.S., Liu, X.M., Wang, X.Q., Liu, H.L. and Wang, W. (2019) Interpretation of regional-scale distribution of high Hg in soils of karst area in southwest China. Geochemistry-Exploration Environment Analysis 19(3), 289-298.

Obrist, D., Agnan, Y., Jiskra, M., Olson, C.L., Colegrove, D.P., Hueber, J., Moore, C.W., Sonke, J.E. and Helmig, D. (2017) Tundra uptake of atmospheric elemental mercury drives Arctic mercury pollution. Nature 547(7662), 201-204.

Qiu, G., Feng, X., Wang, S., Fu, X. and Shang, L. (2009) Mercury distribution and speciation in water and fish from abandoned Hg mines in Wanshan, Guizhou province, China. Science of the Total Environment 407(18), 5162-5168.

Qiu, G.L., Feng, X.B., Wang, S.F. and Mao, T.F. (2006) Mercury contaminations from historic mining to water, soil and vegetation in Lanmuchang, Guizhou, southwestern China. Science of the Total Environment 368(1), 56-68.
Ravel, B. and Newville, M. (2005) ATHENA, ARTEMIS, HEPHAESTUS: data analysis for X-ray absorption spectroscopy using IFEFFIT. J Synchrotron Radiat 12(Pt 4), 537-541.
Reis, A.T., Lopes, C.B., Davidson, C.M., Duarte, A.C. and Pereira, E. (2014) Extraction of mercury water-soluble fraction from soils: An optimization study. Geoderma 213, 255-260.
Santos-Frances, F., Garcia-Sanchez, A., Alonso-Rojo, P., Contreras, F. and Adams, M. (2011) Distribution and mobility of mercury in soils of a gold mining region, Cuyuni river basin, Venezuela. Journal of Environmental Management 92(4), 1268-1276.
Santos, J.C.B.d., Le Pera, E., Oliveira, C.S.d., Souza Júnior, V.S.d., Pedron, F.d.A., Corrêa, M.M. and Azevedo, A.C.d. (2019) Impact of weathering on REE distribution in soil-saprolite profiles developed on orthogneisses in Borborema Province, NE Brazil. Geoderma 347, 103-117.
Schwesig, D. and Matzner, E. (2000) Pools and fluxes of mercury and methylmercury in two forested catchments in Germany. Science of the Total Environment 260(1-3), 213-223.
Shaheen, S.M. and Rinklebe, J. (2018) Vanadium in thirteen different soil profiles originating from Germany and Egypt: Geochemical fractionation and potential mobilization. Applied Geochemistry 88, 288-301.
Silva-Filho, E.V., Machado, W., Oliveira, R.R., Sella, S.M. and Lacerda, L.D. (2006) Mercury deposition through litterfall in an Atlantic forest at Ilha Grande, Southeast Brazil. Chemosphere 65(11), 2477-2484.
Smith, C.N., Kesler, S.E., Blum, J.D. and Rytuba, J.J. (2008) Isotope geochemistry of mercury in source rocks, mineral deposits and spring deposits of the California Coast Ranges, USA. Earth and Planetary Science Letters 269(3-4), 399-407.
Soleh Setiyawan, A., Effendi, A.J., Lestari, V., Irsyad, M., Dwi Ariesyady, H., Nastiti, A., Roosmini, D. and Sonny Abfertiawan, M. (2020) Optimizing soil washing remediation of mercury contaminated soil using various washing solutions and solid/liquid ratios. E3S Web of Conferences 148, 05004.
Sun, J.L., Zou, X., Ning, Z.P., Sun, M., Peng, J.Q. and Xiao, T.F. (2012) Culturable microbial groups and thallium-tolerant fungi in soils with high thallium contamination. Science of the Total Environment 441, 258-264.
Sun, Z.Y., Wen, X.F., Wu, P., Liu, Y. and Pan, Q.Z. (2019) Excessive Degrees and Migration Characteristics of Heavy Metals in Typical Weathering Profiles in Karst Areas. Earth and Environment 47(1), 50-56(In Chinese with English abstract).
Teršič, T., Biester, H. and Gosar, M. (2014) Leaching of mercury from soils at extremely contaminated historical roasting sites (Idrija area, Slovenia). Geoderma 226-227, 213-222.
Terzano, R., Santoro, A., Spagnuolo, M., Vekemans, B., Medici, L., Janssens, K., Goettlicher, J., Denecke, M.A., Mangold, S. and Ruggiero, P. (2010) Solving mercury (Hg) speciation in soil samples by synchrotron X-ray microspectroscopic techniques. Environmental Pollution 158(8), 2702-2709.
Tsui, M.T., Blum, J.D. and Kwon, S.Y. (2020) Review of stable mercury isotopes in ecology and biogeochemistry. Science of the Total Environment 716, 135386.
Wang, J., Shaheen, S.M., Anderson, C.W.N., Xing, Y., Liu, S., Xia, J., Feng, X. and Rinklebe, J. (2020) Nanoactivated Carbon Reduces Mercury Mobility and Uptake by Oryza sativa L: Mechanistic Investigation Using Spectroscopic and Microscopic Techniques. Environmental Science & Technology 54(5), 2698-2706.
Wang, S.F., Feng, X.B., Qiu, G.L., Wei, Z.Q. and Xiao, T.F. (2005) Mercury emission to atmosphere from Lanmuchang Hg-Tl mining area, Southwestern Guizhou, China. Atmospheric Environment 39(39), 7459-7473.
Wang, X., Bao, Z., Lin, C.-J., Yuan, W. and Feng, X. (2016) Assessment of Global Mercury Deposition through Litterfall. Environmental Science & Technology 50(16), 8548-8557.
Wang, X., Yuan, W., Feng, X., Wang, D. and Luo, J. (2019) Moss facilitating mercury, lead and cadmium enhanced accumulation in organic soils over glacial erratic at Mt. Gongga, China. Environmental Pollution 254(Pt A), 112974.

Wiederhold, J.G., Skyllberg, U., Drott, A., Jiskra, M., Jonsson, S., Bjorn, E., Bourdon, B. and Kretzschmar, R. (2015) Mercury isotope signatures in contaminated sediments as a tracer for local industrial pollution sources. Environmental Science & Technology 49(1), 177-185.
Wu, X., Wei, Y., Wang, J., Wang, D., She, L., Wang, J. and Cai, C. (2017) Effects of soil physicochemical properties on aggregate stability along a weathering gradient. Catena 156, 205-215.
Xia, J., Wang, J., Zhang, L., Wang, X., Yuan, W., Anderson, C.W.N., Chen, C., Peng, T. and Feng, X. (2021a) Significant mercury efflux from a Karst region in Southwest China - Results from mass balance studies in two catchments. Science of the Total Environment 769, 144892.
Xia, J., Wang, J., Zhang, L., Wang, X., Yuan, W., Zhang, H., Peng, T. and Feng, X. (2021b) Mass balance of nine trace elements in two karst catchments in southwest China. Science of the Total Environment 786, 147504.
Xiao, Q., Dong, Z., Han, Y., Hu, L., Hu, D. and Zhu, B. (2021) Impact of soil thickness on productivity and nitrate leaching from sloping cropland in the upper Yangtze River Basin. Agriculture, Ecosystems & Environment 311, 107266.
Yin, R., Gu, C., Feng, X., Hurley, J.P., Krabbenhoft, D.P., Lepak, R.F., Zhu, W., Zheng, L. and Hu, T. (2016) Distribution and geochemical speciation of soil mercury in Wanshan Hg mine: Effects of cultivation. Geoderma 272, 32-38.
Yin., Feng, X. and Shi, W. (2010) Application of the stable-isotope system to the study of sources and fate of Hg in the environment: A review. Applied Geochemistry 25(10), 1467-1477.
Yu, B., Fu, X., Yin, R., Zhang, H., Wang, X., Lin, C.J., Wu, C., Zhang, Y., He, N., Fu, P., Wang, Z., Shang, L., Sommar, J., Sonke, J.E., Maurice, L., Guinot, B. and Feng, X. (2016) Isotopic Composition of Atmospheric Mercury in China: New Evidence for Sources and Transformation Processes in Air and in Vegetation. Environmental Science & Technology 50(17), 9262-9269.
Zhao, M., Zeng, C., Liu, Z. and Wang, S. (2010) Effect of different land use/land cover on karst hydrogeochemistry: A paired catchment study of Chenqi and Dengzhanhe, Puding, Guizhou, SW China. Journal of Hydrology 388(1-2), 121-130.

Graphical Abstract

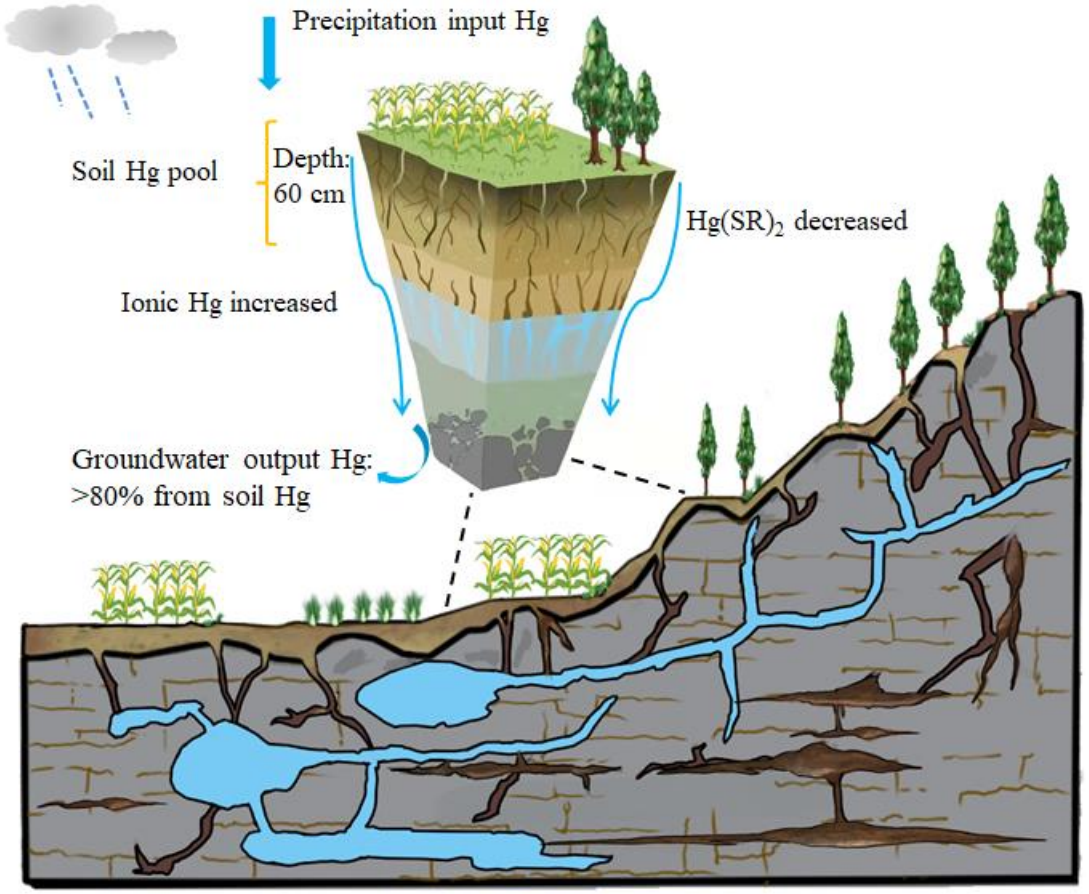

List of Figures

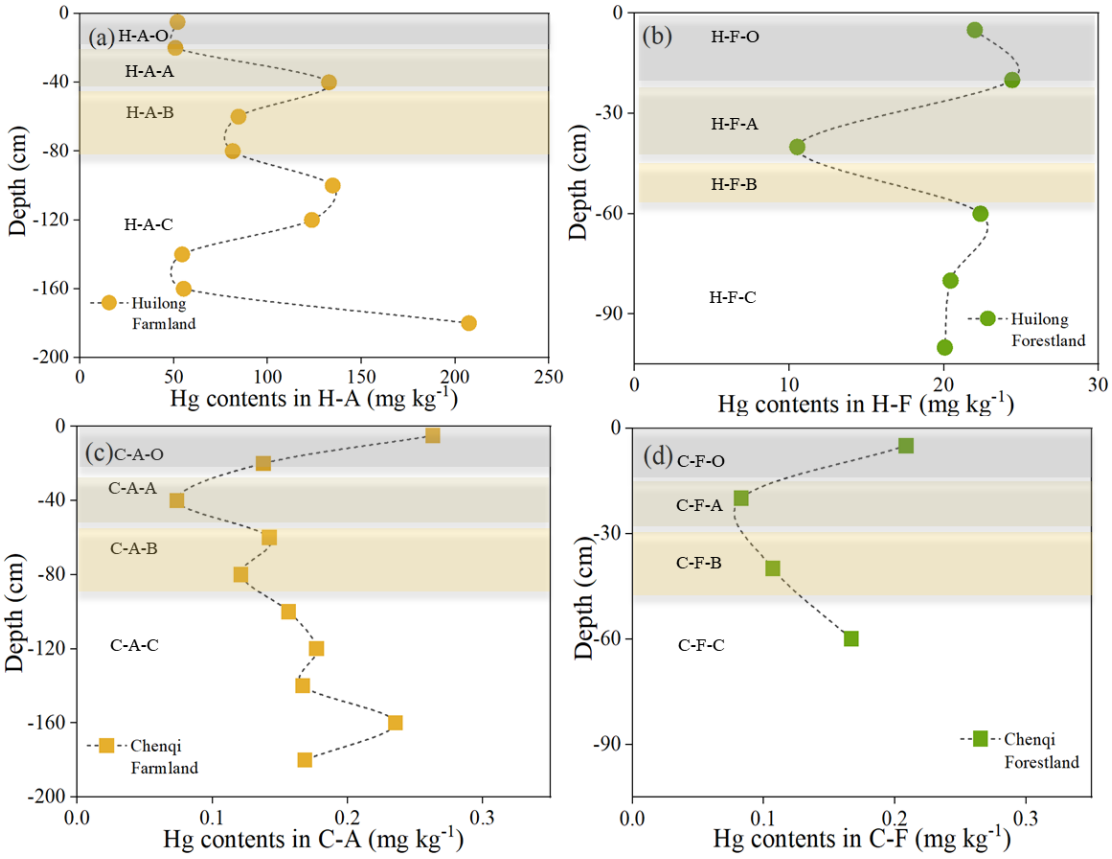

Fig. 1 Distribution of soil Hg content in the farmland (a) and forestland (b) sections of the Huilong catchment and in the farmland (c) and forestland (d) sections of the Chenqi catchment. H-A-O, H-A-A, H-A-B and H-A-C (C-A-O, C-A-A, C-A-B and C-A-C) represent the plough layer, leaching layer, deposition layer and parent layer of farmland soil profile in the Huilong (Chenqi) catchment, respectively; H-F-O, H-F-A, H-F-B and H-F-C (C-F-O, C-F-A, C-F-B and C-F-C) represent the organic matter layer, leaching layer, deposition layer and parent layer of forestland soil profile in the Huilong (Chenqi) catchment, respectively.

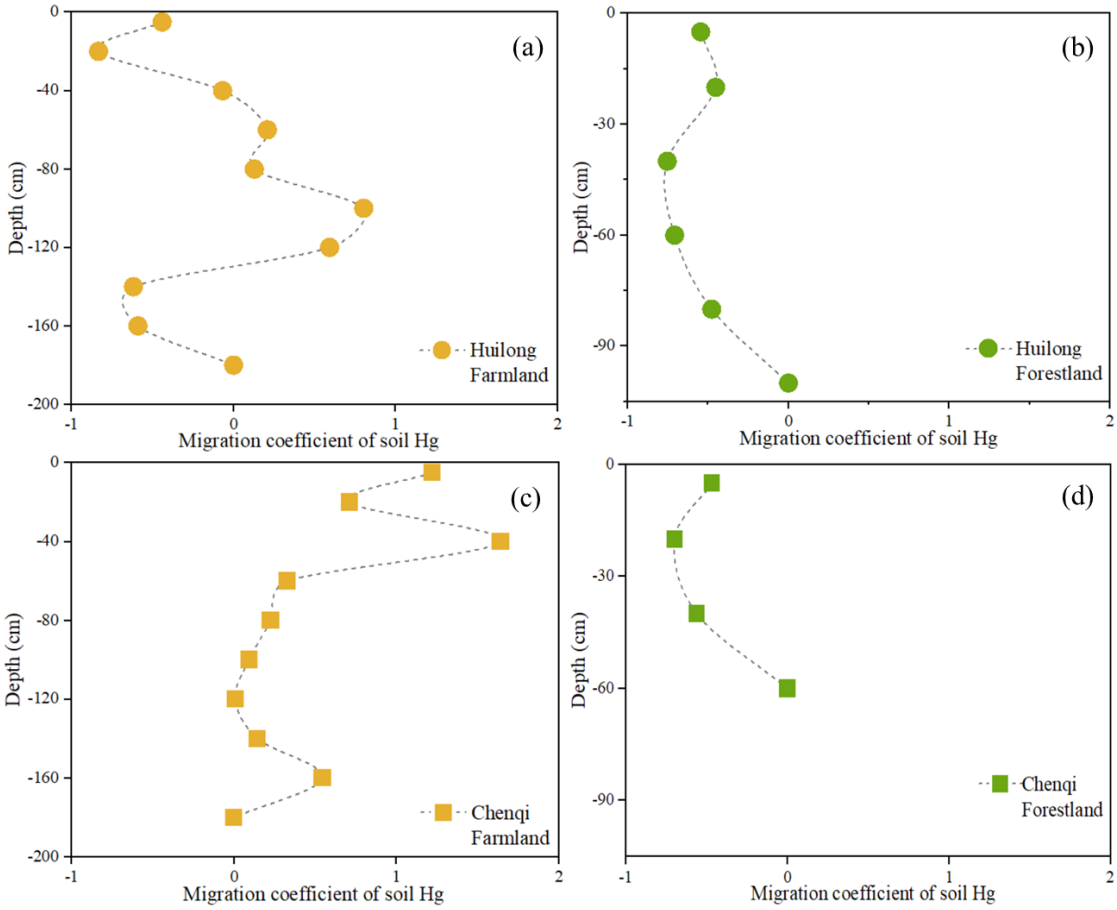

Fig. 2 Migration coefficient (*MC*) of soil Hg in Huilong and Chenqi catchments.

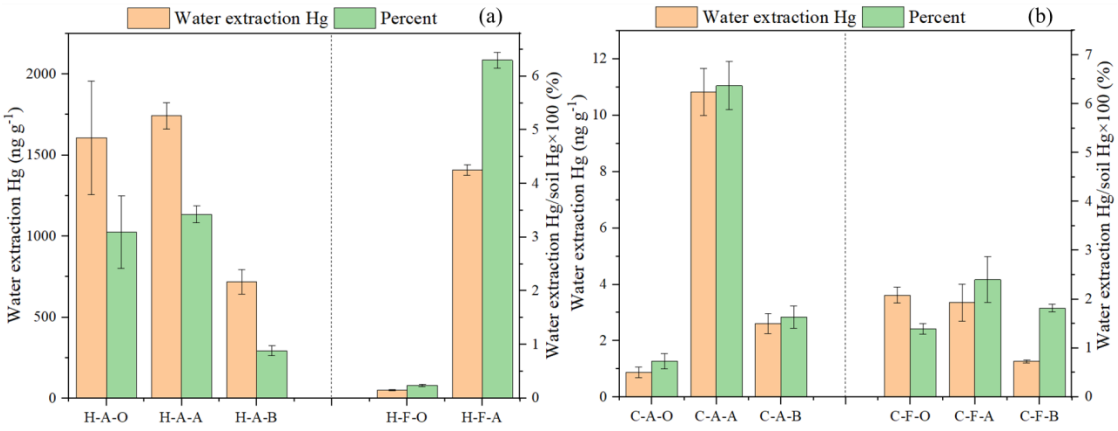

Fig. 3 Distribution of water extracted soil Hg and its percentage out of the total Hg in the farmland and forestland soil profiles of the two catchments. H-A-O, H-A-A and H-A-B (C-A-O, C-A-A and C-A-B) represent the plough layer, leaching layer and deposition layer of farmland soil profile in the Huilong (Chenqi) catchment, respectively; H-F-O and H-F-A (C-F-O and C-F-A) represent the organic matter layer and leaching layer of forestland soil profile in the Huilong (Chenqi) catchment, respectively. C-F-B represents the deposition layer of the forest soil profile in the Chenqi catchment.

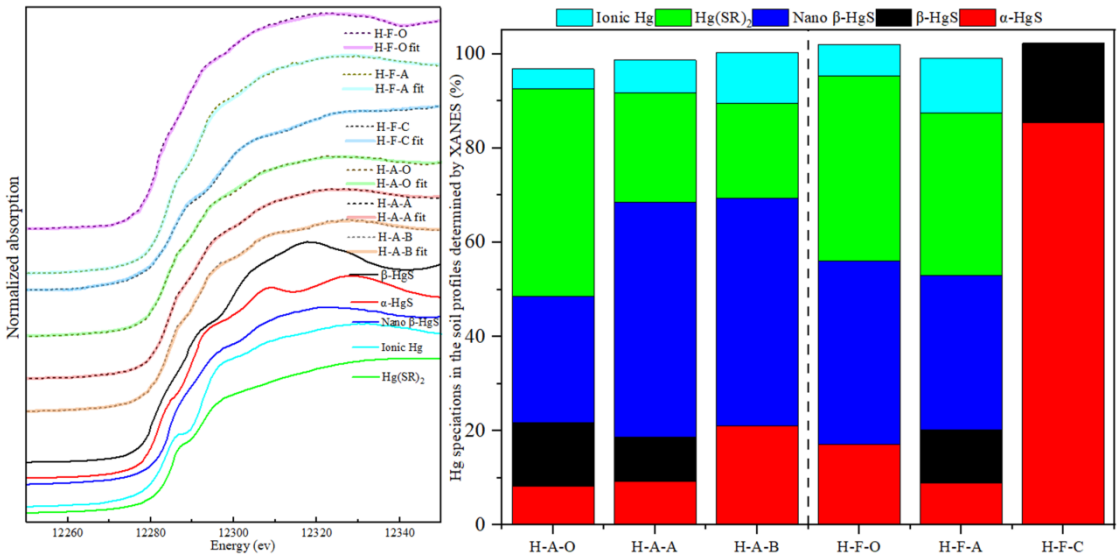

Fig. 4 XANES analysis of soil Hg in farmland and forestland profiles in the Huilong catchment. H-A-O, H-A-A and H-A-B represent the plough layer, leaching layer, and deposition layer of farmland soil profile in the Huilong catchment, respectively; H-F-O, H-F-A and H-F-C represent the organic matter layer, leaching layer and parent layer of forestland soil profile in the Huilong catchment, respectively.

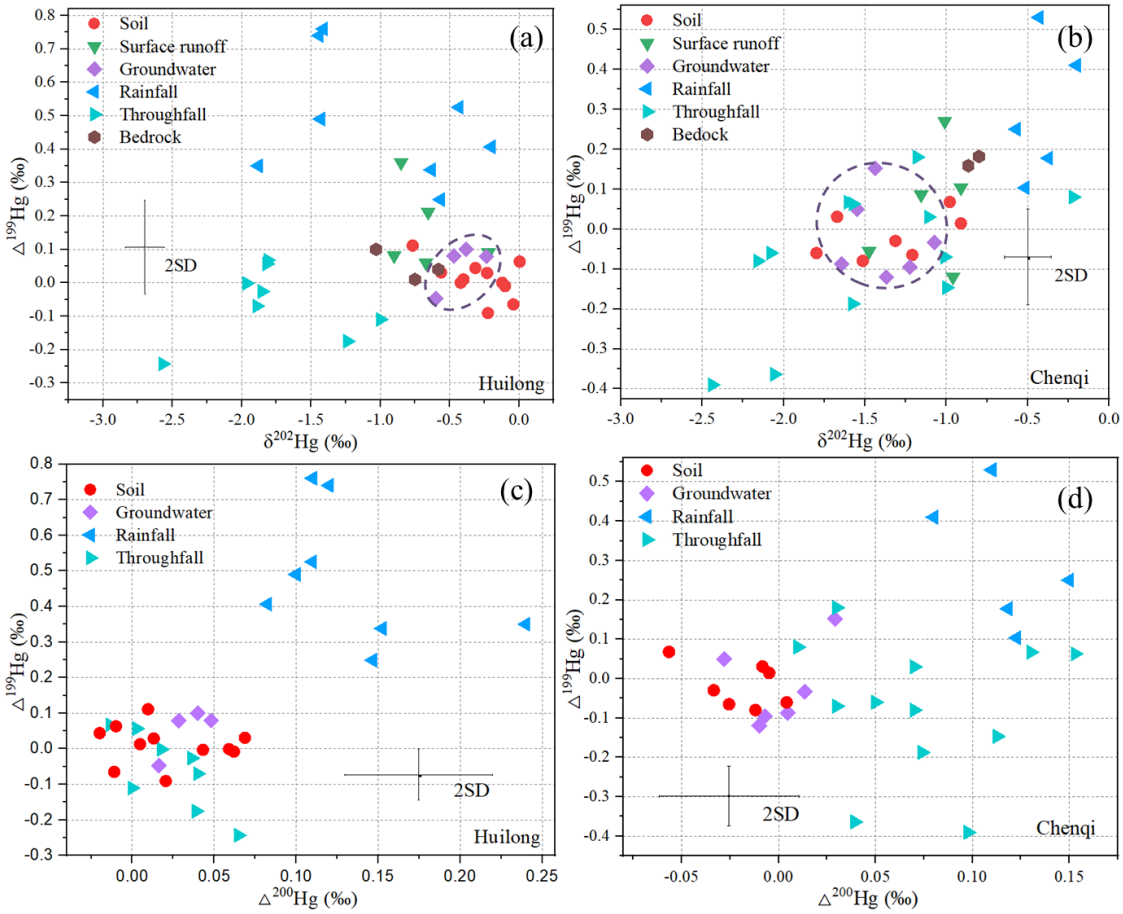

Fig. 5 The Hg isotope composition of environmental media in Huilong and Chengqi catchments.

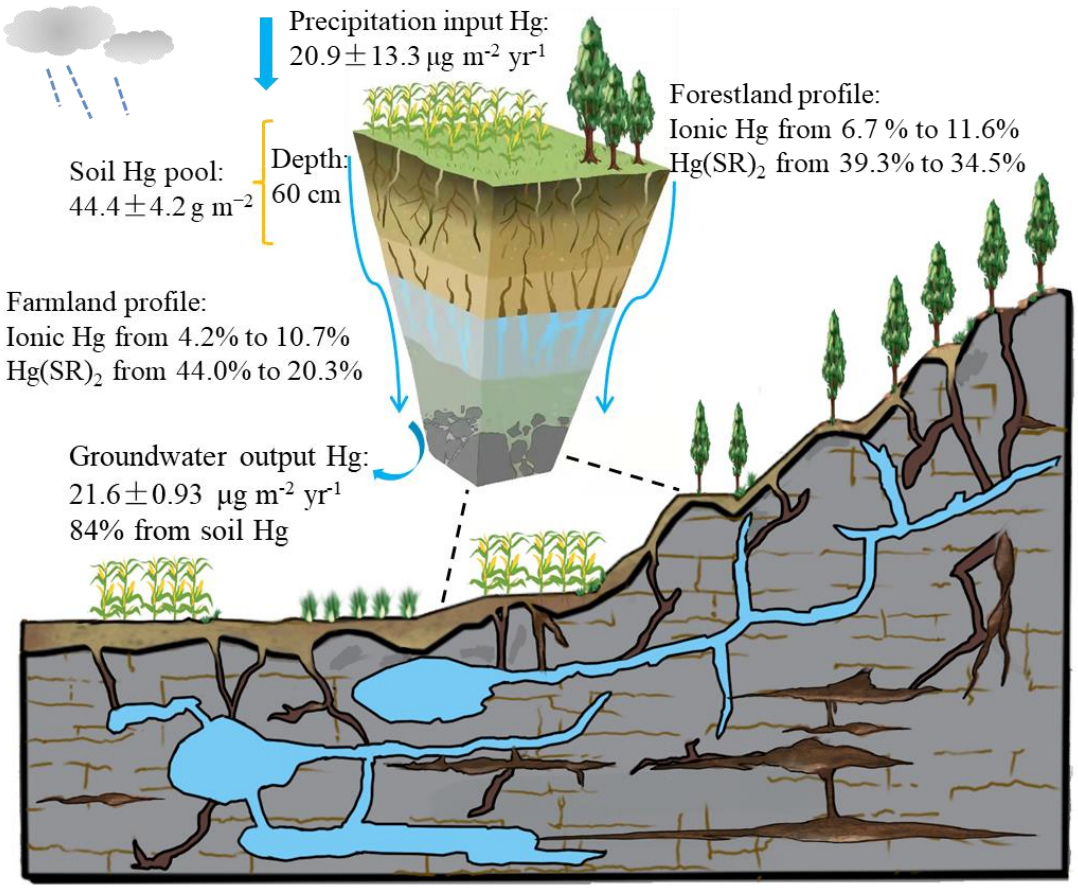

Fig. 6 Schematic illustration of Hg migration and transformation in farmland and forestland soil profiles in Huilong catchment. The central soil column diagram was modified from Chorover et al. (2007) and data of Hg input from precipitation and Hg output through runoff were adopted from Xia et al. (2021a).